

# The Influence of Argon, Air and Hydrogen Gas on Thermal Conductivity of Gas Diffusion Layers and Temperature Gradients in PEMFCs

Robert Bock<sup>a</sup>, Bjørnar Hamre<sup>b</sup>, Morten Onsrud<sup>c</sup>, Håvard Karoliussen<sup>a</sup>, Frode Seland<sup>d</sup> and Odne S. Burheim<sup>a</sup>

<sup>a</sup>Department of Energy and Process Engineering, Norwegian University of Science and Technology (NTNU), NO-7491 Trondheim, Norway

<sup>b</sup>Trondheim City Urban Development, NO-7004 Trondheim, Norway

<sup>c</sup>NORSIRK AS, NO-0663 Oslo, Norway

<sup>d</sup>Department of Materials Science and Engineering, Norwegian University of Science and Technology, NO-7491 Trondheim, Norway

Gas diffusion layers (GDL) in fuel cells have to satisfy a range of conflicting demands. They must deliver good mass transport, but also good electrical and thermal transport. The thermal conductivity of two GDLs was measured with either hydrogen or argon present inside the pores. The results show an increase of up to 19% with regard to the thermal conductivity for the Freudenberg H1410 GDL with hydrogen present in the pores as opposed to measurements with air present. The thermal conductivity in the Sigracet 10BA GDL was also enhanced, with an increase of 15% with hydrogen present in the pores. This correlates with the thermal conductivity of hydrogen gas, which is higher than that of air. Furthermore, the results suggest that the GDL materials have a lower thermal conductivity with argon gas present in the pores. The thermal conductivity for Freudenberg H1410 increased from  $0.119 \pm 0.011 \text{ WK}^{-1}\text{m}^{-1}$  for air to a thermal conductivity of  $0.140 \pm 0.015 \text{ WK}^{-1}\text{m}^{-1}$  for hydrogen gas at a compaction pressure of 10 bar. The thermal conductivity of Sigracet 10BA increased from  $0.30 \pm 0.05 \text{ WK}^{-1}\text{m}^{-1}$  for air to a thermal conductivity of  $0.32 \pm 0.03 \text{ WK}^{-1}\text{m}^{-1}$  for hydrogen gas at a compaction pressure of 10 bar. These results suggest that the gas present in the pores has a significant influence on the thermal conductivity of the GDL. Additionally, a 2D thermal model has been constructed to represent the impact of the results on the temperature distribution inside a fuel cell.

## Introduction

Renewable energy technology and clean fuels like hydrogen are gaining a significant amount of attention in present research efforts. They are the key to reducing the need for fossil hydrocarbon-based energy production and transport. Fuel cells are energy conversion devices that can convert chemical energy into electricity using hydrogen gas. These fuel cells can be reversed to produce hydrogen using electricity via electrolysis. Many renewable electricity sources (e.g., wind and solar) are intermittent, and in many cases peak production does not align with peak consumption. One way to store this excess renewable energy would be as hydrogen through the process of water

electrolysis. The stored hydrogen can again be recovered with a fuel cell when demands peak. This way fuel cells can be an energy buffer and help to stabilize power systems based on renewable energy sources. More than 50% of the energy released within a Proton Exchange Membrane Fuel Cell (PEMFC) is dissipated in the form of heat (1). To further develop and optimize the PEMFC technology, the understanding and management of this heat is a crucial factor. Determining the heat distribution in a PEMFC helps to comprehend its kinetics and water management (2). To represent the temperature distribution correctly, precise thermal conductivity values of the subcomponents of the PEMFC are needed. Traditionally, the thermal conductivity has been determined for the porous subcomponents on the anode and cathode side in the PEMFC when saturated with air. However, in operational mode, the PEMFC is saturated with hydrogen gas, not air, on the anode side. Hydrogen gas has a thermal conductivity seven times higher than that of air. This work aims to reveal the importance of determining the thermal conductivity for porous materials under the same circumstances as they would experience in an operational PEMFC, as suggested by Ramousse et al. (2007) (3). The effect of a hydrogen saturated anode region on the temperature profile within the PEMFC is explored by determining how the thermal conductivity of air, argon, and hydrogen gas in a porous material affect the total thermal conductivity of that region. Measurements with argon gas are used as a reference to demonstrate the effect hydrogen has on the thermal conductivity of GDLs.

### Thermal conductivity

As the PEMFC produces electricity from hydrogen and oxygen, the chemical energy that cannot be converted into electrical work will show up as heat. The heat is produced mainly near the middle of the membrane electrode assembly (MEA), where the formation of water occurs. Ohmic resistance and overpotentials produce the majority of the heat within the PEMFC (4). The heat is transported through the fuel cell (in the normal direction to the sheets of MEA) to the cooling channels that are needed to control the operating temperature of the whole cell. This leads to temperature gradients inside the fuel cell that are far from the often applied isothermal assumption used in many early simulations. To accurately predict fuel cell temperature distributions, the thermal conductivities of all fuel cell components are required.

Vie and Kjelstrup (2004) were among the first to experimentally report a large temperature gradient inside the PEMFC. They found temperature differences of 5 K or more between the membrane surface near the centre of the fuel cell and the gas channels. They estimated a thermal conductivity of  $0.18 \text{ WK}^{-1}\text{m}^{-1}$  for the Nafion 115 membrane and values of  $0.2 \pm 0.1 \text{ WK}^{-1}\text{m}^{-1}$  for the ETEK ELAT gas diffusion layer (GDL) and catalyst layer combined (platinum loading of  $0.1 \text{ mg cm}^{-2}$ ). The temperature gradient indicated that there was a great need to carry out more research on the thermal conductivity of materials used in the PEMFC. (5)

An experimental setup much like the one used in this work was used by Khandelwal et al. (2006) to determine the through-plane thermal conductivity of dry Nafion, various diffusion media, the catalyst layer, and the thermal contact resistance between diffusion media and a metal plate as a function of temperature and pressure. The through-plane dry Nafion thermal conductivity was determined to be  $0.16 \pm 0.03 \text{ WK}^{-1}\text{m}^{-1}$  at room temperature, and decreased to  $0.13 \pm 0.02 \text{ WK}^{-1}\text{m}^{-1}$  at  $65^\circ\text{C}$ . The GDL thermal conductivity was found to be a function of polytetrafluoroethylene (PTFE) content and the method in which the GDL was manufactured. For SIGRACET diffusion media they

measured the thermal conductivity to be  $0.48 \pm 0.09 \text{ WK}^{-1}\text{m}^{-1}$  for untreated and  $0.22 \pm 0.04 \text{ WK}^{-1}\text{m}^{-1}$  for 20 wt% PTFE treated material, respectively. The Toray carbon paper GDL thermal conductivity was measured to be  $1.80 \pm 0.27 \text{ WK}^{-1}\text{m}^{-1}$  at  $26^\circ\text{C}$  and decreased to  $1.24 \pm 0.19 \text{ WK}^{-1}\text{m}^{-1}$  at  $73^\circ\text{C}$ . The thermal contact resistance between the Toray carbon paper and an aluminium bronze material was determined to drop from  $6.7 \cdot 10^{-4}$  to  $2.0 \cdot 10^{-4} \text{ m}^2\text{KW}^{-1}$  when the compaction pressure, an external mechanical pressure applied in the through-plane direction of the material, increased from 4 to 22 bar. The equivalent thermal conductivity of a  $0.5 \text{ mg cm}^{-2}$  platinum loaded catalyst layer (CL) was estimated to be  $0.27 \pm 0.05 \text{ WK}^{-1}\text{m}^{-1}$ . A one-dimensional analytical model was used to estimate the temperature drop in the fuel cell components. A maximum temperature drop of 3-4 K could be expected for a  $200 \mu\text{m}$  thick SIGRACET GDL at  $1.0 \text{ Acm}^{-2}$ . (6)

Ramousse et al. (2008) concluded that the majority of values for thermal conductivity encountered in the earlier literature were highly overestimated. They made an analytical and an experimental approach, the latter with a measurement setup using the same concept as the test rig described in this work. Because of the nature of the transfer of heat in porous and fibrous materials it is difficult to estimate the effective thermal conductivity of samples consisting of non-woven carbon felts. (3)

Burheim et al. (2010) determined the thermal conductivity of wetted Nafion membranes and SolviCore GDLs. Their experimental methodology was applied to this work and is explained there in detail. Thermal conductivities of Nafion membranes were measured *ex situ* at  $20^\circ\text{C}$  to be  $0.177 \pm 0.008$  and  $0.254 \pm 0.016 \text{ WK}^{-1}\text{m}^{-1}$  for dry and maximally wetted membranes respectively. For the dry GDL at 4.6, 9.3 and 13.9 bar compaction pressures, the thermal conductivity was found to be 0.27, 0.36 and  $0.40 \text{ WK}^{-1}\text{m}^{-1}$  and the thermal contact resistivity to the apparatus was determined to be 2.1, 1.8 and  $1.1 \cdot 10^{-4} \text{ m}^2\text{KW}^{-1}$ , respectively. It was shown that the thermal contact resistance between two GDLs is negligible compared to the apparatus' thermal contact resistivity. For a humidified GDL, the thermal conductivity increased by up to 70% due to a residual liquid saturation of 25%. (2)

The contact resistance between the GDL material and adjacent surfaces/layers was deemed as important to explore as the effective thermal conductivity by Sadeghi et al. (2010). Experiments were performed on Toray carbon papers with 78% porosity and 5% PTFE under a cyclic compressive load. Results showed a significant hysteresis in the loading and unloading cycle data for total thermal resistance, thermal contact resistance, effective thermal conductivity, thickness, and porosity. It was found that after five loading-unloading cycles, the geometrical, mechanical, and thermal parameters reached a "steady-state" condition and remained unchanged. The contact resistance was found to be the dominant contributor to the total resistance. However, the contact resistance depends largely on the material and surface of the adjacent layers. (7)

In a subsequent study Sadeghi et al (2011) found that in-plane thermal conductivity differs significantly from the through-plane direction due to the anisotropic microstructure of the GDL. A novel test bed that allowed separation of in-plane effective thermal conductivity and thermal contact resistance in GDLs was introduced. Measurements were performed using Toray carbon paper TGP-H-120 samples with varying PTFE content at a mean temperature of  $65\text{--}70^\circ\text{C}$ . The in-plane effective thermal conductivity was found to remain approximately constant at  $17.5 \text{ WK}^{-1}\text{m}^{-1}$  over a wide range of PTFE content, and its value was about 12 times higher than that for through-

plane conductivity. (8)

More in-plane measurements were carried out on different GDL materials by Teertstra et al. (2011). A parallel thermal conductance technique was used to determine the in-plane thermal conductivity. Conductivity values were measured at a mean sample temperature of 70°C for six different material types and two different orientations in order to quantify the effect of PTFE content on thermal conductivity and to reveal any anisotropic behaviour. The in-plane thermal conductivity was found to be at least ten times that of the through-plane thermal conductivity. The results varied from a minimum of 3.54 WK<sup>-1</sup>m<sup>-1</sup> to a maximum value of 15.1 WK<sup>-1</sup>m<sup>-1</sup> for various samples and configurations tested in that study, with an uncertainty between 1% and 2% for all the cases investigated. (9) Thermal conductivity changes over a large temperature range was researched by Zamel et al. (2011). Using the thermal capacitance method to experimentally measure the through-plane thermal conductivity of Toray carbon paper for a temperature range from -50 to +120°C, it was found that the thermal conductivity increases with higher temperatures. (10)

An earlier study by the same research group found that the in-plane thermal conductivity decreased at higher temperatures; therefore, the thermal expansion of the carbon fibres is a direction dependent quantity (11). Burheim et al. (2014) measured the thermal conductivity of different catalyst layers (CLs) both in dry and moist conditions. It was found that the thermal conductivity of the dry CLs and the CLs with low water content was between 0.07–0.11 WK<sup>-1</sup>m<sup>-1</sup> when 5-15 bar compaction pressure was used to compress the layers. When adding water, it was observed that it only influenced the thermal conductivity when the water content was significantly beyond the capacity of the polymer. This means that the extra water, when the ionomer is oversaturated, caused the change in thermal conductivity found in the CL. The CLs tested were found to compress almost irreversibly and to be uncompressible beyond a compaction pressure of 10 bar. (12)

Burheim et al. (2015) also studied the composition and thermal properties of the GDL. By using X-ray computed tomography (XCT) and scanning electron microscopy (SEM) they found that a micro porous layer (MPL) coated GDL acts like a three-layered structure consisting of MPL on one side, GDL on the other side, and a composite region in the middle where the two materials are infused with each other. It was found that the MPL-GDL-composite region must have a much larger thermal conductivity than the other two; therefore, the temperature drop over the composite layer may be neglected compared to the other two layers. The pure MPL layer was found to have a significantly lower thermal conductivity than the other two layers. Therefore, the MPL should be integrated into the GDL to reduce the temperature deviation in the PEMFC. (13)

In an experimental study Bock et al. (2018) manufactured pure composite material of GDL and MPL to investigate these claims. They found that the thermal conductivity for GDLs with high thermal conductivity to begin with was lowered by the addition of MPL material, where GDLs with low thermal conductivity show an increased thermal conductivity after treatment with MPL. (14)

Two review articles by Cindrella et al. (2009) and Zamel et al. (2013) focus on GDLs and offer more insight on this scientific field and how it has advanced over the recent years (15, 16). Burheim and Pharoah (2017) published a review article where they discuss the case of heat production in PEMFC and the upcoming challenge of

removing this heat with fuel cells becoming more effective energy converters (17).

Burheim (2017) also reviewed the influence of thermal conductivity on temperature profiles inside a PEMFC. He compared available data from literature and implemented these into a model to obtain temperature profiles. (4)

### Thermal models

It is of great importance to understand the thermal behaviour of a PEMFC for different designs and under the various operating conditions to be able to accurately predict the temperature distribution in new PEMFCs. Because experimental determination of the temperature distribution is invasive and has significant costs associated with it, thermal modeling is favoured for quickly covering many different parameter variations.

Nguyen and White (1993) were among the first in PEMFC modeling while investigating the effectiveness of various humidification designs (18).

Wöhr et al. (1998) were first with modeling in the through-plane direction while investigating dehumidification effects of changing current densities. They modeled stacks of several cells, lacking some of the detail inside the MEA that later studies showed. (19)

Rowe and Li (2001) developed a one-dimensional through-plane model, but they neglected the differences in properties of GDL, MPL, GDL-MPL composite and catalyst layer and treat them all as one (20).

Djilali et al. (2002) published a one-dimensional non-isothermal model. They found that non-uniform temperature and pressure distributions have a large impact on the predicted liquid water and vapour fluxes in the GDL of the PEMFC, which they also treated as one homogeneous layer in the model. (21)

Berning et al. (2002) reported a comprehensible three-dimensional model (22).

Ju et al. (2004) published with a single phase, non-isothermal model with focus on the correct expressions for various heat generation sources. They modeled with rather high GDL thermal conductivities of  $0.5 - 3 \text{ WK}^{-1}\text{m}^{-1}$  and neglected the thermal gradients of catalyst layer, microporous layer and the recently discussed intermediate region consisting of MPL and GDL together. This suggested the importance of knowing the thermal conductivity of the GDL is for managing the coupled thermal and water management inside a PEMFC. (23)

Pasaogullari et al. (2004) included an MPL in their PEMFC model on the cathode side (24). Bapat et al. (2007) focussed on the anisotropic thermal conductivity of the GDL, but not on the through plane thermal conductivity (25).

A brief review was published by Kandlikar and Lu (2009) on thermal management issues. They reported thermal conductivities for all layers to be considered, membrane, CL, MPL and GDL combined, and the bipolar plate in a review of the heat transport inside a PEMFC. (26)

Recently, Burheim and Pharoah (2017) pointed out the different temperature distributions of a 1D model when taking all of the PEMFC layers into consideration (17).

Collectively, emphasis has been made on the future research needs of thermal gradients and heat aspects both experimentally and numerically.

In a separate extensive review, Burheim (2017) discusses current knowledge about thermal conductivities. He introduces a 2D model to show what influence parameters found in various research publications have on the temperature profile through the MEA. (4) The model used here is similar to the one in his work.

## Experimental

### Thermal conductivity

The measurements of thermal conductivity for this work were performed ex-situ in a custom-built measurement rig that is depicted in Figure 1. Its design is based on a previous work in our group (2). The rig applies the "constant heat flux" method where the apparatus sends a constant heat flux through a cylindrical geometry that is symmetrical on top and bottom. The heat flux is generated by thermoelectric Peltier modules on either side, one heating, the other cooling, to obtain a stable heat flux through the steel cylinders. Samples and stacks of different thickness can be studied, their thickness is recorded by two Mitutoyo micrometers. Through a pneumatic setup compression forces of up to 23 bar can be applied progressively throughout testing, while the change in thickness is monitored.

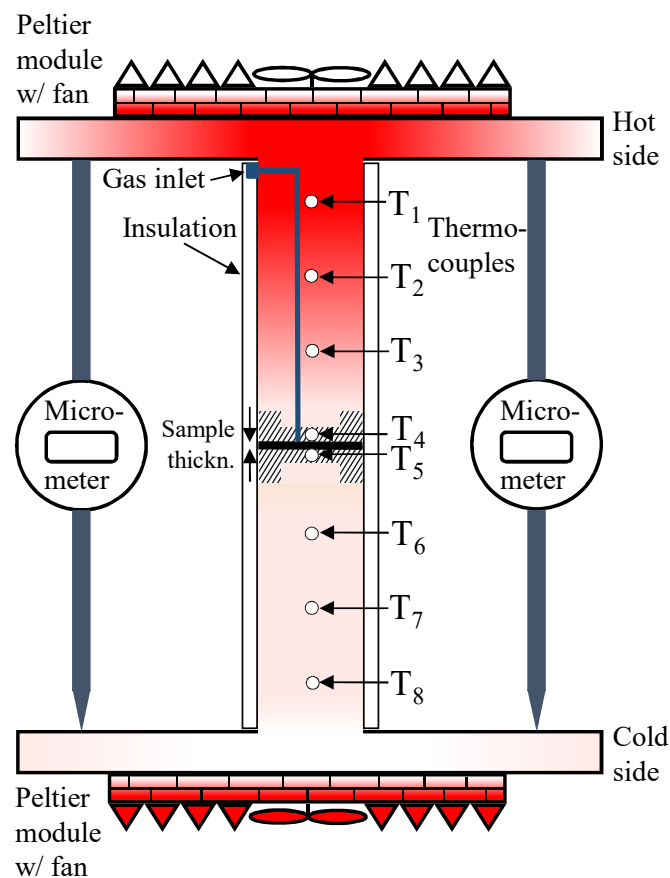


Figure 1. Sketch of the measurement rig, modified from Bock et al. (14)

To measure the thermal conductivity the three other variables from Fourier's law

must be obtained. In its one-dimensional form Fourier's law reads

$$q_x = -\kappa \frac{dT}{dx} \quad [1]$$

where  $q_x$  is the heat flux in x-direction through the sample,  $\kappa$  is the thermal conductivity of interest and  $dT$  is the temperature change over the sample thickness  $dx$ . For this rig the sample thickness is measured with the mentioned micrometers and the temperature difference over the sample is recorded via two thermocouples that are placed inside an aluminium cap on either side of the sample. Aluminium has been chosen for its high thermal conductivity so that the temperature measured close to the sample surface can be assumed to be very close to the temperature on the sample surface (see Figure 2 in (2)). For the determination of the heat flux through the sample, the device contains a further three thermocouples placed equally apart both in the upper and the lower steel cylinders. With the knowledge of the thermal conductivity of steel, the distance between the thermocouples and the measured temperature difference between them, the heat flux towards the sample can be calculated. To ensure the main part of heat transport is in the wanted direction a heat cap was designed and fitted around the steel cylinders for thorough insulation against the surroundings. Thus thermal conductivity could be calculated via

$$\kappa = -q_x \frac{\Delta x}{\Delta T}. \quad [2]$$

With the known temperature difference across the sample the thermal resistance  $r_{th}$  can be obtained. Because of the position of the thermocouples the thermal resistance will also contain some contact resistance  $r_{contact}$  between rig and sample. To decouple the thermal resistance in the sample,  $r_{sample}$ , from the contact resistance the same material is measured at different thicknesses either by purchasing accordingly or by stacking several samples. When stacking several samples, the sample-sample contact resistance can be neglected as reported in (2). When plotting these thermal resistances against the sample thickness (as seen in Figure 2), a linear relation is obtained. Here, the inverse slope of a common trendline gives the thermal conductivity and the intersection of the trendline with the y-axis at zero thickness gives a value for the total sample-rig thermal contact resistance, between sample and the upper and lower cylinder, hence  $2r_{contact}$ .

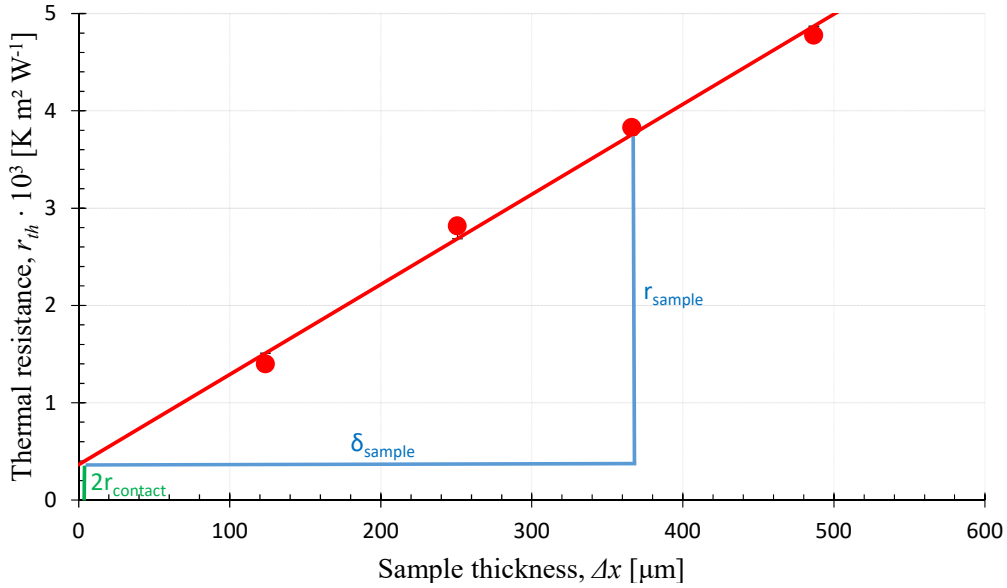


Figure 2. Example for plot of thermal resistance against sample thickness

The novelty in these measurements is the possibility to change the gas type the samples experience under testing. A small gas channel inside the rig can be used to saturate the sample with a chosen gas at atmospheric pressure. This works for all compaction pressures. The temperature in the sample is kept as close to room temperature as possible. The gas travels a long distance at a low flow speed through tubes maintained at room temperature; therefore, the sample and gas should be at room temperature. Only the thermal conductivity of the gas affects the results, not the internal energy of the gas as it enters the sample. Hydrogen gas was chosen to reveal what the actual thermal conductivity of a GDL on the anode side under operating conditions is. These results were compared with results obtained with air inside the sample. To confirm the influence of the gas change on thermal conductivity, argon was chosen as a third gas, as it has a lower thermal conductivity than air and would supposedly change the thermal conductivity in the opposite direction to hydrogen. Hydrogen gas was supplied by a small commercial electrolyzer (Proton OnSite G400, USA). A gas bottle supplied argon (AGA, Norway). Both gases were throttled to atmospheric pressure and not humidified. Table I gives an overview of the thermal conductivities of the materials and gases used in the experiment.

TABLE I. Values of thermal conductivity for the used gases and solids (27)

| Material / substance                   | $\kappa$ at 25°C<br>[ $\text{Wm}^{-1}\text{K}^{-1}$ ] |
|--|---|
| <i>gaseous at atmospheric pressure</i> |   |
| Air                                    | 0.024   |
| Argon                                  | 0.018   |
| Hydrogen                               | 0.168   |
| Oxygen                                 | 0.024   |
| <i>solid</i>                           |   |
| Aluminium, pure                        | 205   |
| Copper                                 | 401   |
| Platinum                               | 70  |
| Steel, stainless (AISI 316)            | 16  |
| Steel (AISI 1095, 1% carbon)           | 45  |

The two GDLs chosen for measurement are Freudenberg H1410 and Sigracet 10 BA. They are readily available commercial GDLs with very different thermal conductivities. Freudenberg H1410 has a reportedly low through-plane thermal conductivity of  $0.111 \pm 0.009 \text{ WK}^{-1}\text{m}^{-1}$ , while Sigracet 10 BA is reported to have a much higher through-plane thermal conductivity of  $0.30 \pm 0.02 \text{ WK}^{-1}\text{m}^{-1}$ , both at around 10 bar compaction pressure (28, 29).

### Modeling

COMSOL Multiphysics was used to model the heat flow inside a PEMFC. A two-dimensional model was used to visualise the impact of the taken measurements. The model does not claim to give an accurate representation of the temperature distribution in a working PEMFC, but rather an indication as to the importance of including the acquired values in future models.

Heat is produced near the middle of the MEA close to the membrane. It must be led out of the PEMFC to avoid overheating the membrane and to ensure the overall efficiency of the PEMFC. The geometry of the modeled part of the MEA is shown in Figure 3.

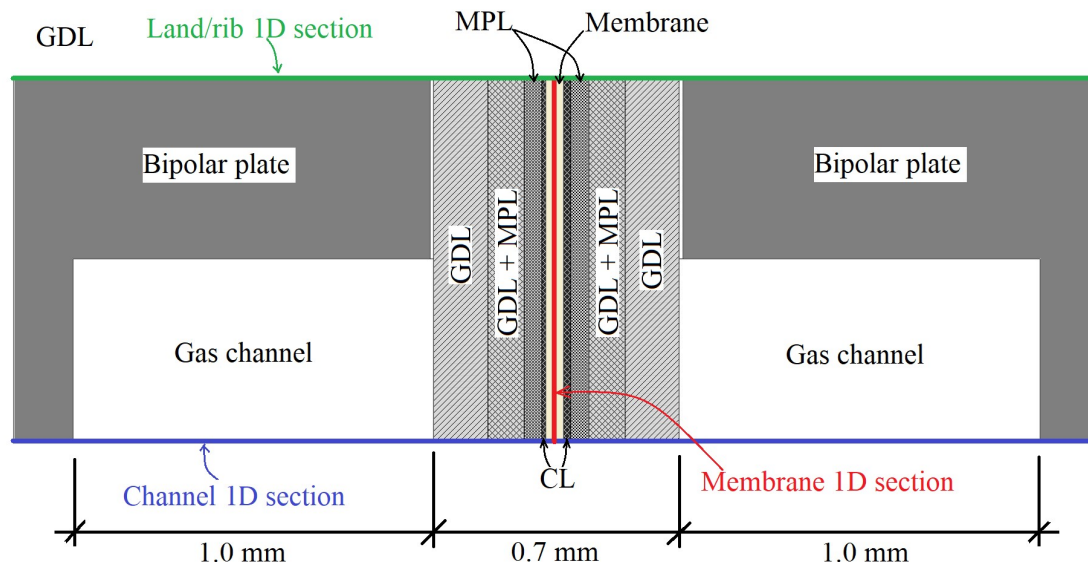


Figure 3. MEA geometry with coloured sections to show the base of the 1D models calculated in COMSOL

The modeling area is a section of a larger PEMFC and is symmetrically cut from the PEMFC. The area outside the model repeats what is seen in the model. The different materials are given individual properties (e.g. the thermal conductivity of the GDL differs from that in the MPL as seen in Table II).

**TABLE II.** Thermal conductivities used in COMSOL model. In-plane  $\kappa$  values have been set to 10 times the value of through-plane  $\kappa$  in GDLs.(8, 9) \*values measured in this work at 10 bar compaction pressure.

| <b>Material</b>     | <b><math>\kappa</math> (through-plane)<br/><math>\text{WK}^{-1}\text{m}^{-1}</math></b> | <b><math>\kappa</math> (in-plane)<br/><math>\text{WK}^{-1}\text{m}^{-1}</math></b> | <b><math>\Delta x</math><br/><math>\mu\text{m}</math></b> | <b>ref.</b> |
|---------------------|---|--|---|-------------|
| Bipolar plates      | 20  | 20   |   | (30)        |
| Air                 | 0.024   | 0.024  | 1000  | (27)        |
| Argon               | 0.016   | 0.016  | 1000  | (27)        |
| Hydrogen            | 0.168   | 0.168  | 1000  | (27)        |
| Freudenberg H1410   |   |  |   |             |
| Air-saturated       | 0.114   | 1.14   | 150   | [*]         |
| Argon-saturated     | 0.108   | 1.08   | 150   | [*]         |
| Hydrogen-saturated  | 0.141   | 1.41   | 150   | [*]         |
| Sigracet 10BA       |   |  |   |             |
| Air-saturated       | 0.299   | 2.99   | 150   | [*]         |
| Argon-saturated     | 0.293   | 2.93   | 150   | [*]         |
| Hydrogen-saturated  | 0.319   | 3.19   | 150   | [*]         |
| MPL-GDL integration | 15  | 15   | 100   | (13)        |
| MPL                 | 0.18  | 0.18   | 50  | (31)        |
| Anode CL            | 0.18  | 0.18   | 10  | (12)        |
| Cathode CL          | 0.18  | 0.18   | 20  | (12)        |
| Membrane            | 0.25  | 0.25   | 50  | (32)        |

As the thermal conductivity of the MPL-GDL composite area has not been tested when saturated with gasses different from air, an assumption is made as to how the gas affects it. Because of the density of the infused parts and the much higher thermal conductivity there, it is assumed that the thermal conductivity of the gas will influence this area at a much smaller scale than in the GDL-only area. The effect of the thermal conductivity of the gas is therefore assumed negligible in this composite region and left out of the COMSOL model. In the gas channel there are two heat transfer mechanisms modeled. Heat diffusion is applied in the entire channel, but close to the walls of the bipolar plate and close to the GDL on the opposing side a  $50 \mu\text{m}$  boundary layer is defined, where both heat convection and heat diffusion are applied. A  $10 \mu\text{m}$  air/gas gap was introduced to account for thermal contact resistance (TCR) between the GDL and bipolar plates around  $320 \mu\text{m}$  away from the center of the MEA; this applies to the land/rib section only. The through-plane and in-plane thermal conductivities differ much in GDL materials. In-plane thermal conductivities are assumed ten times greater here than through-plane thermal conductivities in the results, according to measurements by Sadeghi et al. (2011) and Teertstra et al. (2011) (8, 9). All thermal conductivity values for GDLs listed in Table II are values at 10 bar compaction pressure. The compaction pressure varies in the MEA from higher compaction pressure under the land/rib to lower compaction pressure in the gas channel of the bipolar plate. This small difference in compaction pressure is not accounted for in the model.

## Results

### Thermal conductivity

The measured thermal conductivities under the influence of the different gasses are presented in Table III. Both GDL materials show a lower thermal conductivity when saturated with argon gas compared to air,  $-13\%$  for Freudenberg and  $-4\%$  for Sigracet GDL at 10 bar compaction pressure. The effect is stronger for higher compaction pressures. When saturated with hydrogen gas, both GDL materials show a higher thermal

conductivity than for air, 18% for Freudenberg and 7% for Sigracet GDL at 10 bar compaction pressure. This effect seems to be constant over the range of compaction pressures.

**TABLE III.** Thermal conductivity values with different gasses for Freudenberg H1410 and Sigracet 10BA

| Compaction pressure [bar] | Freudenberg H1410 with                           |  |   | Sigracet 10BA with                               |  |   |
|---------------------------|--|--|---|--|--|---|
|                           | Air $\kappa$ [WK <sup>-1</sup> m <sup>-1</sup> ] | Argon $\kappa$ [WK <sup>-1</sup> m <sup>-1</sup> ] | Hydrogen $\kappa$ [WK <sup>-1</sup> m <sup>-1</sup> ] | Air $\kappa$ [WK <sup>-1</sup> m <sup>-1</sup> ] | Argon $\kappa$ [WK <sup>-1</sup> m <sup>-1</sup> ] | Hydrogen $\kappa$ [WK <sup>-1</sup> m <sup>-1</sup> ] |
| 3                         | 0.108 ± 0.013                                    | 0.10 ± 0.02  | 0.125 ± 0.014   | 0.244 ± 0.017                                    | 0.236 ± 0.016                                      | 0.281 ± 0.012   |
| 5                         | 0.111 ± 0.012                                    | 0.099 ± 0.012                                      | 0.132 ± 0.012   | 0.26 ± 0.03                                      | 0.25 ± 0.02  | 0.287 ± 0.008   |
| 10                        | 0.119 ± 0.011                                    | 0.103 ± 0.011                                      | 0.140 ± 0.015   | 0.30 ± 0.05                                      | 0.29 ± 0.02  | 0.32 ± 0.03   |
| 15                        | 0.124 ± 0.012                                    | 0.109 ± 0.009                                      | 0.143 ± 0.013   | 0.33 ± 0.05                                      | 0.32 ± 0.03  | 0.37 ± 0.02   |
| 20                        | 0.128 ± 0.013                                    | 0.112 ± 0.012                                      | 0.148 ± 0.013   | 0.38 ± 0.08                                      | 0.34 ± 0.04  | 0.396 ± 0.012   |
| 23                        | 0.131 ± 0.013                                    | 0.116 ± 0.017                                      | 0.152 ± 0.017   | 0.40 ± 0.08                                      | 0.35 ± 0.04  | 0.44 ± 0.04   |

Thermal conductivity is plotted as a function of compaction pressure in Figure 4 for all materials and gasses. It was expected that  $\kappa$  would increase with pressure for all tested materials.

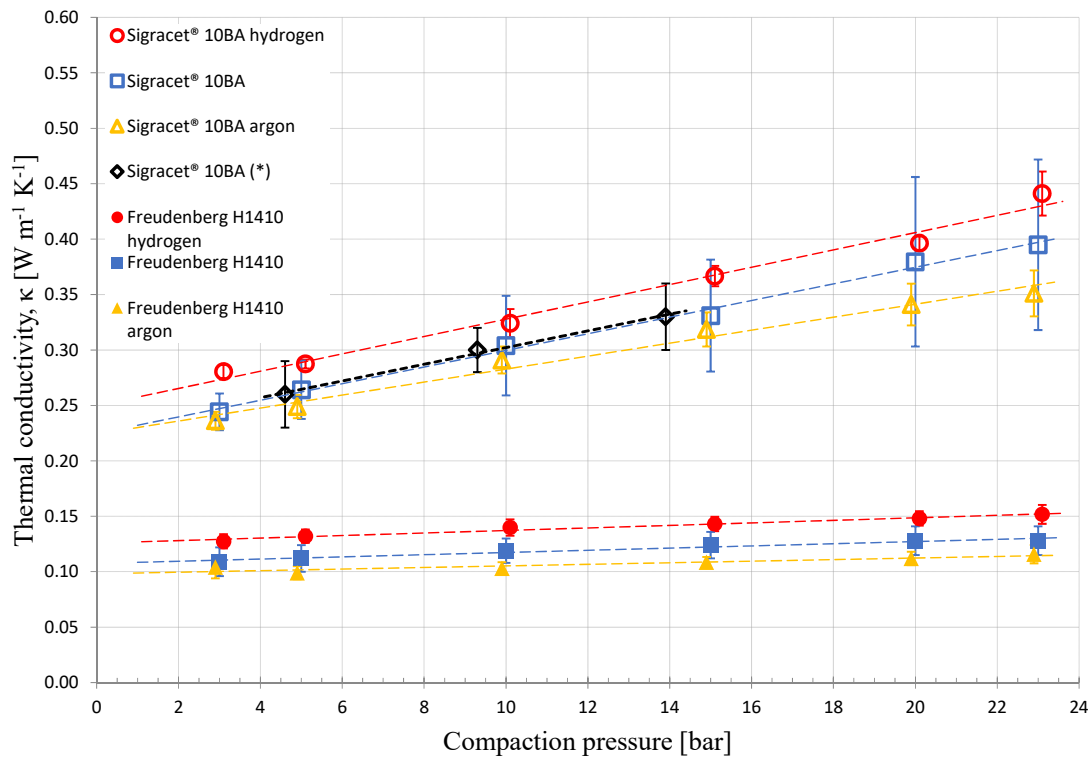


Figure 4. Thermal conductivity as a function of compaction pressure for Sigracet 10BA and Freudenberg H1410 GDLs saturated with air, argon, and hydrogen. \*Literature values (29)

The change towards higher thermal conductivity at higher compaction pressures is more prominent for the Sigracet material than for the Freudenberg GDL. This behaviour does not change when saturated with hydrogen or argon. The gasses have an effect that seems to be constant over the range of compaction pressures. To ascertain the validity of the new measurement rig literature values for Sigracet GDL were included in the plot (29). They show excellent agreement with our measurements when measured with air.

Another plot is presented in Figure 5, where thermal resistance for all the tested materials is shown as a function of the sample thickness at 10 bar compaction pressure. 10 bar is a likely compaction pressure in a PEMFC and used in earlier models.(29) The thermal conductivities  $\kappa$  found here at 10 bar were used as input parameters in the COMSOL modeling section.

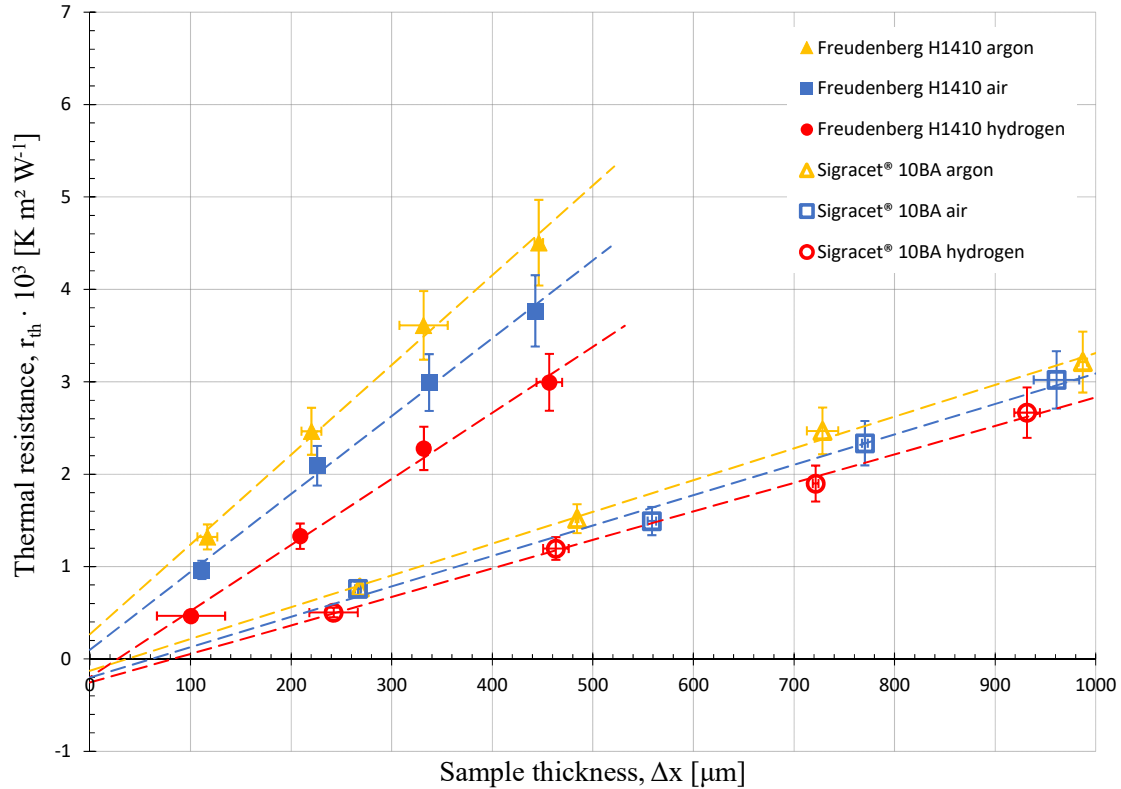


Figure 5. Thermal resistance as a function of thickness at 10 bar for Sigracet 10BA and Freudenberg H1410 GDLs saturated with air, argon, and hydrogen. Thermal conductivities are extracted from the slopes of the respective trendlines.

The slopes of the trendlines shown are readily distinguishable. Their slope gives a value for the average thermal conductivity of the material tested. The difference between the two GDL materials is prominent, but also the gas present in the GDL produces a notable difference in the thermal resistance results. Most notably both GDLs, even though very different in weight, compressibility, and thermal resistance, are affected the same way by the change in atmosphere. Even though the thermal conductivities of the gases are lower than the thermal conductivities of the GDL materials, the high porosity of the GDLs lets the gases take up a large part of the volume and influence the total thermal resistance. This is especially noteworthy as the thermal transport in these porous media is expected to mainly go via solids, that is the carbon fibers and their intersections, where the use of binders further enhances transport. The thermal contact resistance is found by reading off the intercept point of the regression line in Figure 5. Overall, contact resistances are small compared to the total thermal resistance. Four of the six regression lines indicate negative contact resistance. This is due to accuracy limitations when comparing temperatures of two different thermocouples.

The decrease in thermal contact resistance with increasing pressure is visualized in Figure 6. The change in the number of contact points and the total direct contact

area between the carbon material in the GDL and the adjacent surface is responsible for this effect. Thermal contact resistance decreases with rising compaction pressure for GDLs regardless of the gas it contains. However, the overall drop is more significant for GDLs saturated with argon and smaller for GDLs saturated with hydrogen. At low compaction pressures when the porosity of the GDL is highest and the number of contact points between the GDL and its adjacent surface is limited, the thermal conductivity of the gas influences the thermal contact resistance the most. When the compaction pressure increases, a more substantial part of the surface is in direct contact with the carbon material in the GDL and the gas is displaced from the surface. The thermal conductivity of the partly displaced gas will not influence the contact resistance as much for higher compaction pressures. The effect is consistent regardless of what GDL material is used. The coloured boxes indicate the thermal resistance a layer of the respective gas has. When analyzing results at 3 bar compaction pressure, the respective contact resistance results for Sigracet and Freudenberg GDL compare to the calculated value for the air/gas gap. The reason for that is when the materials are barely compressed, and there are few contact points between GDL and the adjacent material, a good portion of the heat transfer goes via diffusion through the gas present. With increasing number of contact points, the influence of the gas becomes less prominent and even negative values are reported due to the mentioned accuracy limitations.

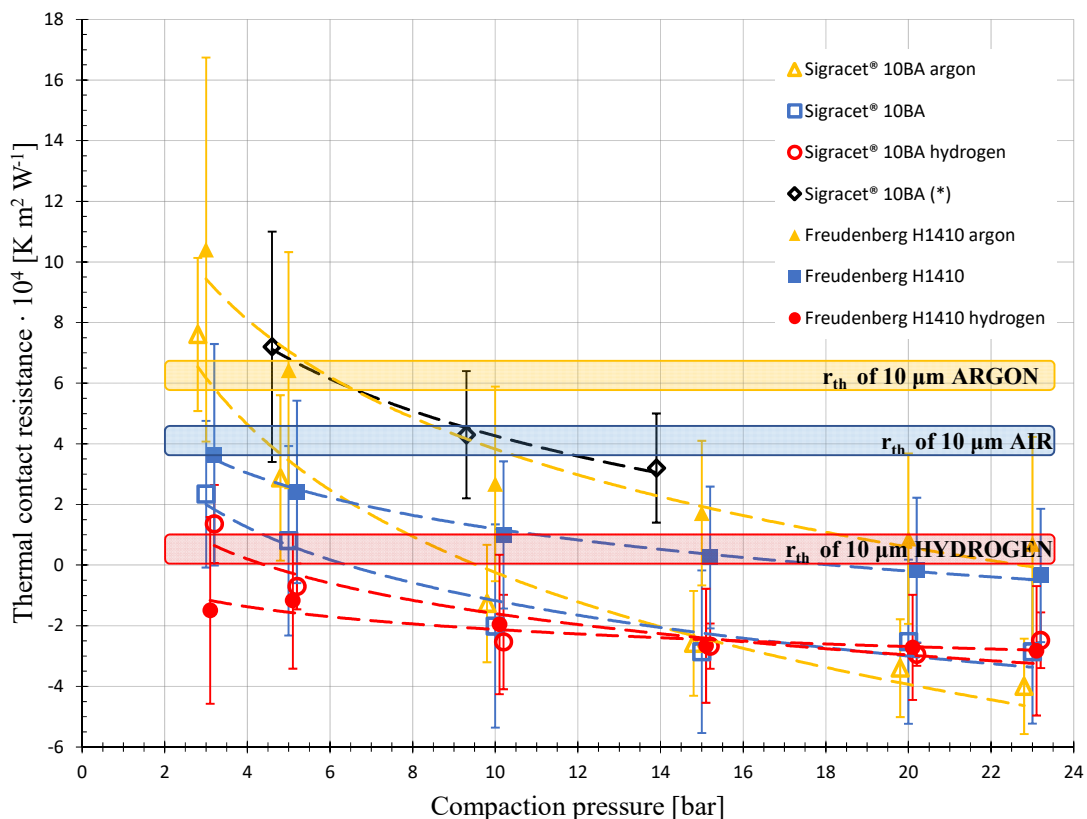


Figure 6. Thermal contact resistance as a function of compaction pressure for Sigracet 10BA and Freudenberg H1410 GDLs saturated with air, argon, and hydrogen. The colour boxes are the thermal resistances of 10  $\mu\text{m}$  of each gas. \*Literature values (2)

## Modeling

The 1D plots in Figure 7a for Sigracet 10BA GDL and Figure 7b for Freudenberg H1410 illustrate the temperatures through the MEA in a straight line where the bipolar

plates are in contact with the GDL. Dotted vertical lines in the plot represent boundaries between two different materials. The figures show the differences in the temperature profiles when hydrogen gas, air, or argon gas is present in the channel and the GDL on the anode side. The heat in the MEA is mostly produced in the boundary region between the catalyst layers and the membrane on the cathode side. The only difference between the curves is the value used for thermal conductivity of the GDL on the anode side and in the gas gap there. The amount of heat transported out of the cell is the same for all three cases.

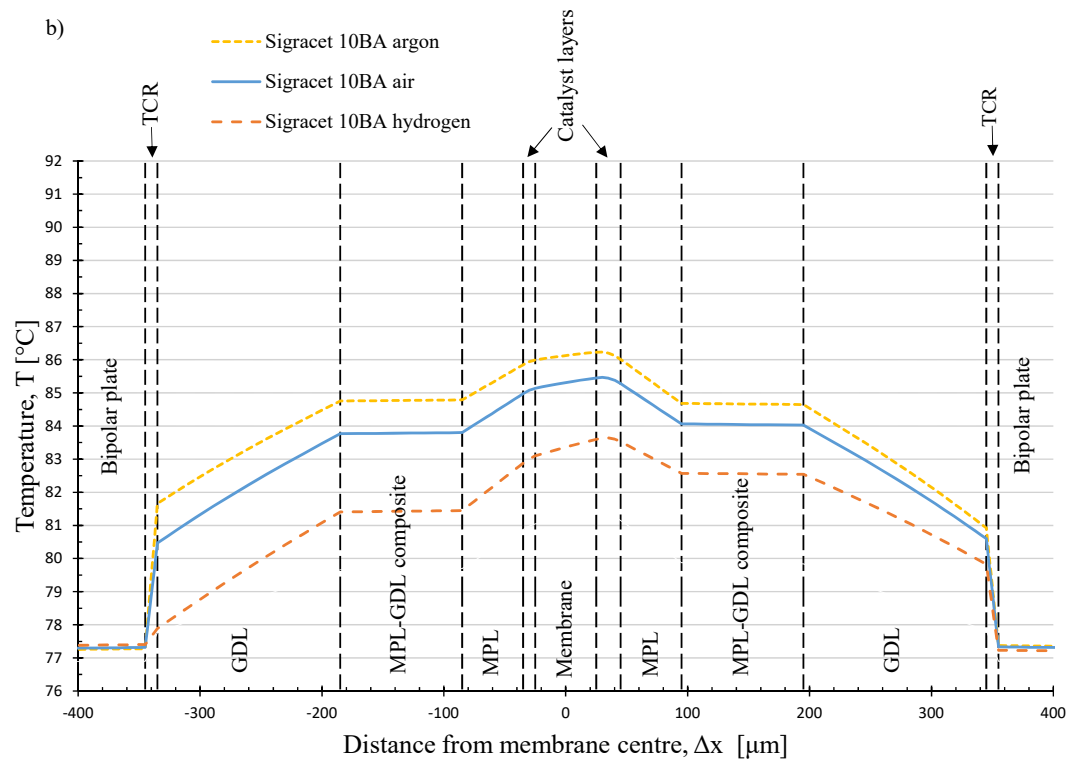
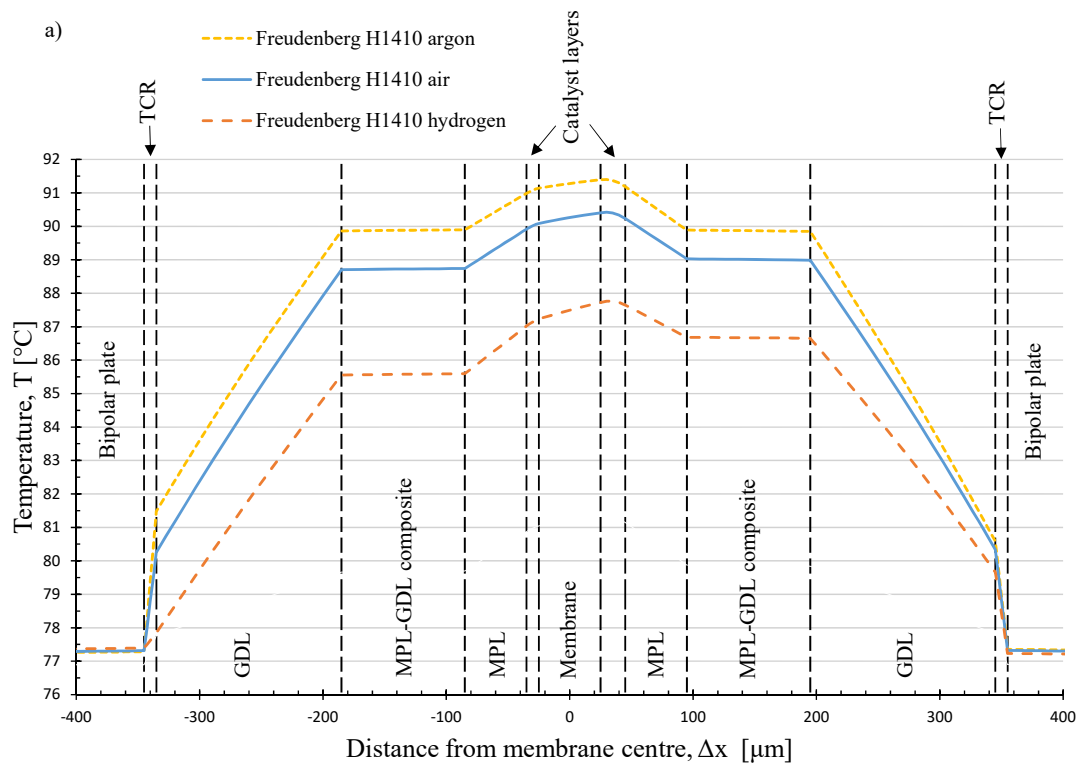


Figure 7. PEMFC land temperature profiles saturated with air, argon, or hydrogen on the anode side. The dotted vertical lines represent the border between different materials in the MEA

Different maximum temperatures can be observed, because thermal resistances on the anode side vary. A hydrogen saturated GDL transports heat away from the centre

of the MEA better than a GDL with air. This also shows up in the temperature gradients. For air, thermal resistance is about equal on anode and cathode side; therefore, the temperature gradients are about equal. When considering the primary heat source near the cathode catalyst layer, the membrane will pose some additional thermal resistance towards the anode side, as observed by the slight temperature difference over the membrane. For hydrogen, temperature differences are larger on the anode side even though the gas reduces thermal resistance. This is because the more significant portion of the heat will now be transported through the anode side due to the lowered thermal resistance, which again results in an increased temperature difference. For argon the behaviour is inverse. Thermal differences are smaller on the anode side because it poses more thermal resistance than the cathode side; therefore, most of the heat will dissipate through the cathode side, which in turn leads to a higher temperature difference there.

The biggest difference in temperature drop between the different cases is in the boundary region between the bipolar plate and the GDL. The thermal contact resistance here influences the total temperature drop considerably. With argon gas in the Freudenberg GDL, the temperature drop from the hottest point to the outer boundary is approximately 14°C. For the case with air in the Freudenberg GDL, the temperature drop is just over 13°C. For the case with hydrogen gas in the Freudenberg GDL, it is just under 11°C, see Figure 7a. This means that the difference between the traditional model, where all GDLs use a thermal conductivity measured with air in the pores, and the case with hydrogen gas in the anode, is over 2°C. A temperature difference of 2°C seems small, but since water vapour pressure is very dependent on temperature, this is considerable. The temperature profiles through the land region of the MEA for a Sigracet 10BA GDL saturated with air, argon, and hydrogen gas is presented in Figure 7b. Here as well, the hydrogen saturated GDL transports heat away from the centre of the MEA better than the GDL with air or argon gas. The Sigracet 10BA GDL has a higher thermal conductivity than the Freudenberg H1410 GDL. Therefore, the temperature drops, from the middle of the MEA to the outer boundary of the model, are smaller for all the cases with Sigracet GDL. For the Sigracet GDL the temperature drop from the hottest point to the outer boundary is 9°C for argon gas, 8.5°C for air, and 6.5°C for hydrogen gas. This gives a difference from the new to the traditional model of about 2°C. The thermal conductivity of the gas could be thought to have less influence on the total thermal conductivity in the Sigracet GDL region. However, the porosity of the Sigracet GDL is higher than that of the Freudenberg GDL, providing more volume for the gas to saturate.

The 1D plots in Figure 8a for the Freudenberg H1410 GDL and Figure 8b for the Sigracet 10BA GDL illustrate the temperatures through the MEA in a straight line through the gas channel. The influence of the gas present on the anode is expected to be larger in these plots because the conductivity of the gas in the channel will influence the results as well as the gas inside the GDL material.

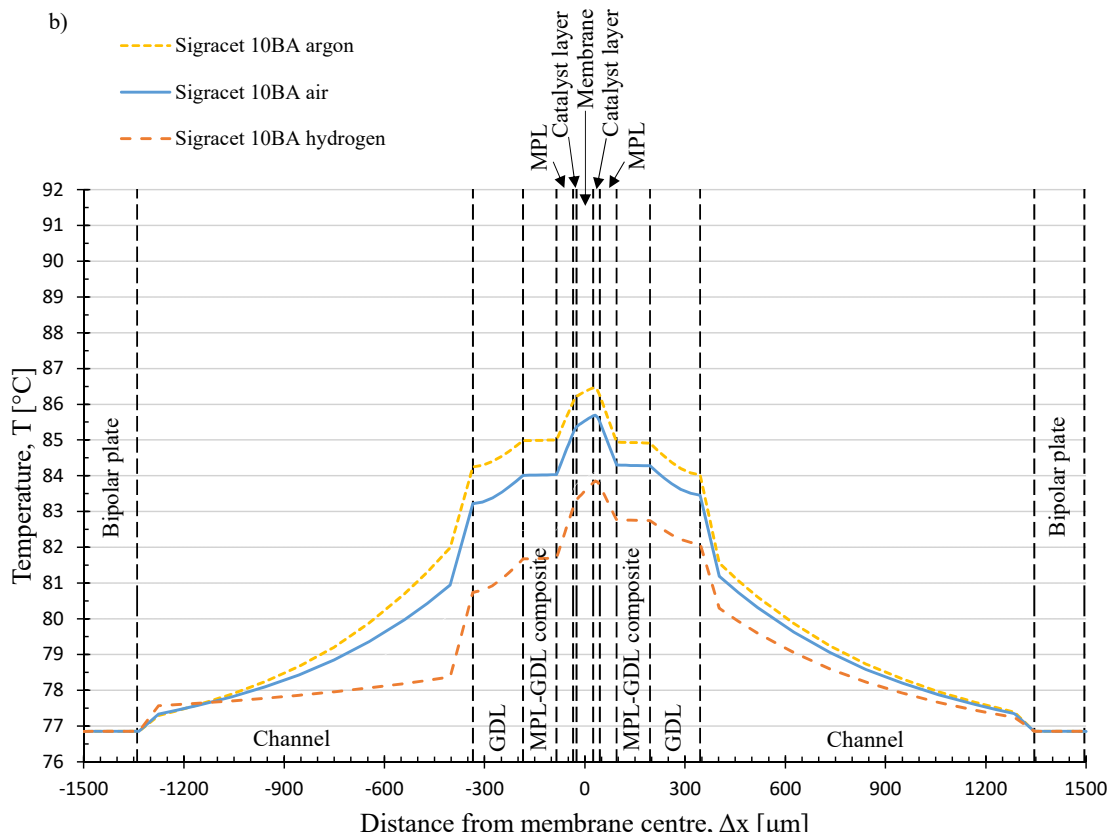
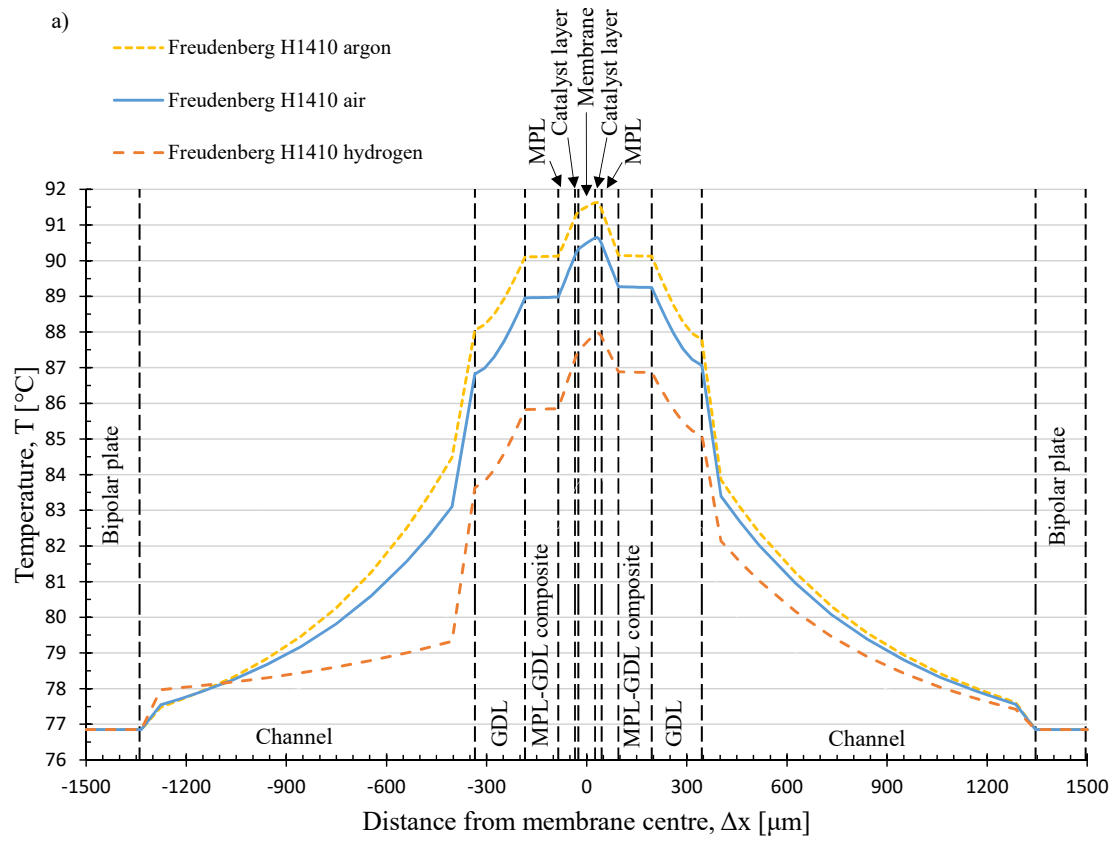


Figure 8. PEMFC channel temperature profiles saturated with air, argon, or hydrogen on the anode side. The dotted vertical lines represent the border between different materials in the MEA

In Figure 8a, a significant temperature drop can be spotted in the gas channel. This temperature difference is highly dependent on the thermal conductivity of the gas in the channel. Therefore, the temperature gradient is much more significant for argon gas and air than for hydrogen gas. The two heat transfer mechanisms modeled in the channel are responsible for the change in temperature gradient there, the model switches from convection and diffusion to diffusion only and vice versa. The total temperature difference from the centre of the MEA to the outer boundary of the model for the Freudenberg H1410 GDL is 15°C for argon gas, 14°C for air, and 11°C for hydrogen gas. A difference of almost 3°C between the simulation with air and the one with hydrogen gas in the channel amounts to about 20% difference. The different cases with the Sigracet 10BA GDL are presented in Figure 8b. The trend is similar to that of the Freudenberg GDL. The higher thermal conductivity in the Sigracet 10BA GDL makes the temperature difference from the centre of the MEA to the outer boundary of the model smaller than for the Freudenberg GDL. The temperature difference is 9.5°C for argon gas, 8.5°C for air, and 7°C for hydrogen gas. That gives a difference of 2.5°C (over 25%) from the simulation with air. The two heat transfer mechanisms are visible here as well.

The temperature in the membrane is crucial for the performance of the PEMFC. If the membrane is overheated it can scorch and become completely disabled from performing its tasks.(33) The temperature seems higher in the middle of the channel when comparing the 1D plots through the channel and bipolar plate. The case where the membrane is hottest is when Freudenberg H1410 GDL is saturated with argon on the anode. Figure 9 shows the temperature profile from the channel to the land of the model as drawn in Figure 3. The temperature difference in the membrane is small. In the land region it is slightly cooler than in the middle of the channel. This is because the thermal conductivity of the bipolar plate is higher than that of the gases in the channel.

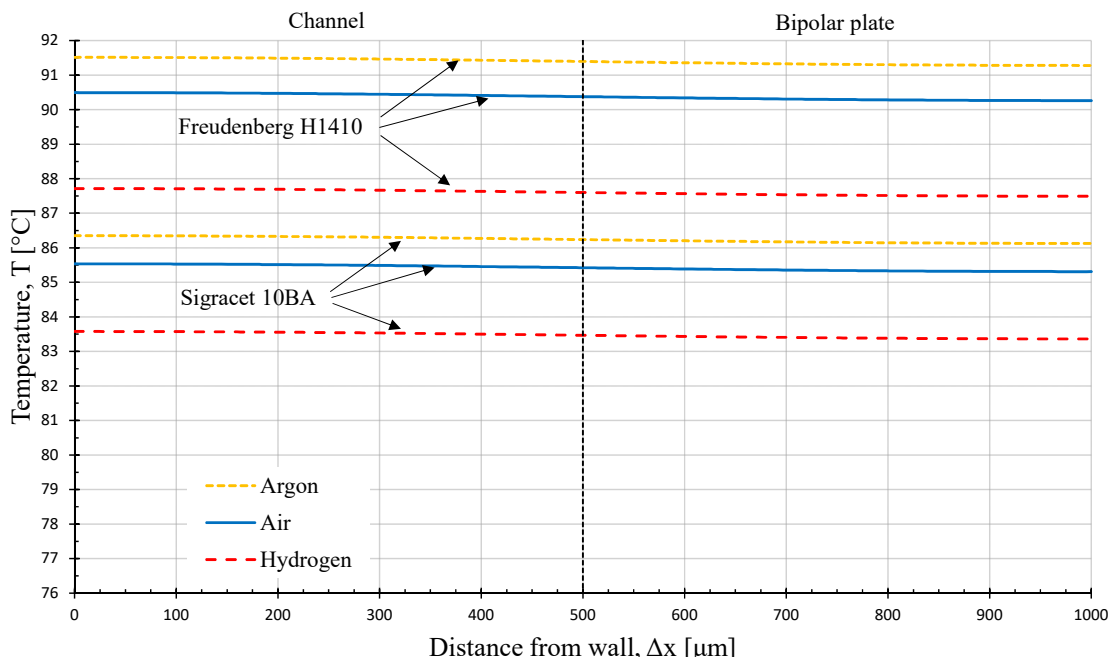


Figure 9. Temperature profile in the middle of a PEMFC membrane from channel to land as shown in red in Figure 3, with Sigracet 10BA and Freudenberg H1410 GDLs saturated with air, argon, and hydrogen on the anode side.

## Discussion

The thermal conductivity of the gas present in a GDL material affects the total thermal conductivity of the GDL region. The measured thermal conductivity for Sigracet 10BA saturated with air fits well with earlier measurements of the same material.(29) This is a strong indication that the measurement rig works appropriately and that the rest of the measured thermal conductivity values are valid results. As expected, the thermal conductivity is higher in a porous region if that region is saturated with gas with a higher thermal conductivity than the reference gas (air), and lower when it is saturated with argon. The difference between the air and hydrogen saturated GDLs is larger than the difference between argon and air GDLs. That is expected as the difference in thermal conductivity is larger for hydrogen and air than for argon and air. The increase in overall thermal conductivity when adding hydrogen has to be attributed to a decreased thermal fiber-to-fiber contact resistance. Similar results are obtained for the addition of solid material to a GDL that sticks to the fiber-to-fiber intersections and decreases contact resistance there. This has been shown in the literature for the addition of water, MPL material and binder material to a GDL (14, 31). The increased heat transport capabilities are then not primarily due to through-pore heat transport but increased fiber-to-fiber heat transport. For addition of argon the fiber-to-fiber contact resistance is slightly increased, respectively.

This is particularly interesting for PEMFC materials, where the anode side is completely saturated with hydrogen gas that has a thermal conductivity seven times higher than air. Thermal conductivity will be different in the anode GDL region from that in the cathode GDL region in a running PEMFC even though the same GDL material is used on both sides. The results provided in Figure 4 show that the effect of the gas present in the GDL is essential to include in any future heat transfer calculations and models regarding PEMFCs.

The thermal resistance in the GDL samples dropped when they were saturated with hydrogen as opposed to air. The thermal resistance increase in the argon saturated GDL points to the same conclusion. Through-plane thermal resistance for GDLs is much greater than in-plane thermal resistance. The direction of the fibers in the GDL and the resulting directional difference in contact points are responsible for that. The results are demonstrating that the thermal resistance of the material dropped each time the compaction pressure increased. The fibers bent and broke under higher compaction pressures and created more through-plane contact points. This trend was consistent regardless of the gas present inside the GDL. However, the drop in thermal resistance and thermal contact resistance with increasing pressure was more abrupt for the GDLs when argon was present. This is because argon gas has an insulating effect that is removed when the sample is compressed and the gas is displaced. The permanent damage to the GDLs from crushed fibers was greater in the lighter and more compressible Sigracet 10BA GDL than in the more compact Freudenberg H1410. This is observed by comparing relative compaction of the materials under the various compaction pressures, as reported in another work.(28) An increase in through-plane contact points was also indicated by the thermal contact resistance results, where the thermal contact resistance dropped with increasing compaction pressure. This points to an increase in contact points between the GDL and the adjacent material as well as inside the sample itself with increasing compaction pressure. The logarithmic trend of the thermal contact resistance as a function of compaction pressure points to the thermal contact resistance approaching zero at infinite compaction pressure. This is a strong argument for the

validity of the results.

The modeling results show that heat transport through the cell is significantly affected by the change of gas in the anode. Different maximum temperatures are the result of varying thermal resistances on the anode side. This also shows up in the temperature gradients. The heat distribution in a working fuel cell is asymmetric. This might call for the somewhat different design of the cooling channels on the anode side than on the cathode side to accommodate the increased heat transport.

### **Conclusion**

This work has contributed to the understanding of heat management in the PEMFC by showing that saturating a porous PEMFC GDL material with hydrogen increases the total thermal conductivity of the GDL region due to the high thermal conductivity of the hydrogen gas as compared to air. The thermal conductivity of the GDLs changed as expected when they were saturated with different gases with different thermal conductivity, as seen in Figure 4. The difference in thermal conductivity is more significant between hydrogen and air than it is between argon and air, something demonstrated by the small distance between the air and argon lines and the more substantial distance between the air and hydrogen lines. The measured thermal conductivity for the Sigracet 10BA GDL fit well with a previous measurement of the same material, a strong indication that the results are valid. The thermal conductivity increased overall by 15 - 20% in the Freudenberg H1410 GDL and 5 - 15% in the Sigracet 10BA GDL when saturating them with hydrogen. Thermal conductivity for Freudenberg H1410 changed from  $0.119 \pm 0.011 \text{ WK}^{-1}\text{m}^{-1}$  for air to a thermal conductivity of  $0.14 \pm 0.015 \text{ WK}^{-1}\text{m}^{-1}$  for hydrogen at a compaction pressure of 10 bar. The thermal conductivity of Sigracet 10BA changed from  $0.30 \pm 0.05 \text{ WK}^{-1}\text{m}^{-1}$  for air to a thermal conductivity of  $0.32 \pm 0.03 \text{ WK}^{-1}\text{m}^{-1}$  for hydrogen at a compaction pressure of 10 bar. Results were obtained for compaction pressures of 3 - 23 bar. The reason the Freudenberg GDL is affected more severely is that it has a thermal conductivity of about half of the Sigracet.

The model results demonstrated a noticeable change in temperature profile through the MEA due to the change in thermal conductivity of the GDL and the gas in the channel on the anode side in the model. This strongly suggests an asymmetric heat distribution and that an updated thermal conductivity value must be implemented in all future models and simulations regarding the temperature profile and transport of heat in the PEMFC to avoid producing misleading results.

In the future, the method used in this work should be adapted to carry out further tests, not only for GDL materials, but for MPLs, multiple layered GDLs, and CLs as well. The possibility to standardize the thermal conductivity change in a porous material due to hydrogen saturation based on the specifications of that material should also be examined. The effect of hydrogen saturation in porous PEMFC should be tested thoroughly at different levels of humidity, as water, the product of the overall reaction in a PEMFC, has been shown to raise the thermal conductivity of the porous regions when compared to dry samples.

### **Acknowledgement**

R. Bock thanks NTNU for providing him with a scholarship.

R. Bock thanks Dr. Jacob Lamb for proof-reading the manuscript as a native English speaker.

The cross-disciplinary ENERSENSE research framework is acknowledged for extra funding.

## References

1. O. S. Burheim, *Engineering Energy Storage*, 1st Edition, Elsevier Academic Press, 2017.
2. O. Burheim, P. Vie, J. Pharoah, S. Kjelstrup, Ex situ measurements of through-plane thermal conductivities in a polymer electrolyte fuel cell, *J. Power Sources* 195 (1) (2010) 249–256.
3. J. Ramousse, S. Didierjean, O. Lottin, D. Maillot, Estimation of the effective thermal conductivity of carbon felts used as pemfc gas diffusion layers, *Int. J. Therm. Sci.* 47 (1) (2008) 1–6.
4. O. Burheim, Review: PEMFC Materials' Thermal Conductivity and Influence on Internal Temperature Profiles, *ECS Transactions* 80 (8) (2017) 509–525.
5. P. J. Vie, S. Kjelstrup, Thermal conductivities from temperature profiles in the polymer electrolyte fuel cell, *Electrochim. Acta* 49 (7) (2004) 1069–1077.
6. M. Khandelwal, M. Mench, Direct measurement of through-plane thermal conductivity and contact resistance in fuel cell materials, *J. Power Sources* 161 (2) (2006) 1106–1115.
7. E. Sadeghi, N. Djilali, M. Bahrami, Effective thermal conductivity and thermal contact resistance of gas diffusion layers in proton exchange membrane fuel cells. part 2: Hysteresis effect under cyclic compressive load, *J. Power Sources* 195 (24) (2010) 8104–8109.
8. E. Sadeghi, N. Djilali, M. Bahrami, A novel approach to determine the in-plane thermal conductivity of gas diffusion layers in proton exchange membrane fuel cells, *J. Power Sources* 196 (7) (2011) 3565–3571.
9. P. Teertstra, G. Karimi, X. Li., Measurement of in-plane effective thermal conductivity in pem fuel cell diffusion media, *Electrochimica Acta* 56 (3) (2011) 1670–1675.
10. N. Zamel, E. Litovsky, S. Shakhshir, X. Li, J. Kleiman, Measurement of in-plane thermal conductivity of carbon paper diffusion media in the temperature range of  $-20\text{ }^{\circ}\text{C}$  to  $+120\text{ }^{\circ}\text{C}$ , *Applied Energy* 88 (9) (2011) 3042–3050.
11. N. Zamel, E. Litovsky, X. Li, J. Kleiman, Measurement of the through-plane thermal conductivity of carbon paper diffusion media for the temperature range from  $-50$  to  $+120\text{ }^{\circ}\text{C}$ , *Int. J. Hydrogen Energy* 36 (19) (2011) 12618–12625.
12. O. S. Burheim, H. Su, H. H. Hauge, S. Pasupathi, B. G. Pollet, Study of thermal conductivity of PEM fuel cell catalyst layers, *Int. J. Hydrogen Energy* 39 (17) (2014) 9397–9408.
13. O. S. Burheim, G. A. Crymble, R. Bock, N. Hussain, S. Pasupathi, A. Du Plessis, S. Le Roux, F. Seland, H. Su, B. G. Pollet, Thermal conductivity in the three layered regions of micro porous layer coated porous transport layers for the PEM fuel cell, *Int. J. Hydrogen Energy* 40 (46) (2015) 16775–16785.
14. R. Bock, A. D. Shum, X. Xiao, H. Karoliussen, F. Seland, I. V. Zenyuk, O. S. Burheim, Thermal conductivity and compaction of gdl-impl interfacial composite material, *Journal of The Electrochemical Society* 165 (7).
15. L. Cindrella, A. Kannan, J. Lin, K. Saminathan, Y. Ho, C. Lin, J. Wertz, Gas diffusion layer for proton exchange membrane fuel cells - a review, *J. Power Sources* 194 (1) (2009) 146–160.
16. N. Zamel, X. Li, Effective transport properties for polymer electrolyte membrane fuel cells - with a focus on the gas diffusion layer, *Progress in energy and combustion science* 39 (1) (2013) 111–146.

17. O. S. Burheim, J. G. Pharoah, A review of the curious case of heat transport in polymer electrolyte fuel cells and the need for more characterization, *Current opinion in electrochemistry*.
18. T. V. Nguyen, R. E. White, A water and heat management model for proton-exchange-membrane fuel cells, *J. Electrochem. Soc.* 140.
19. M. Wöhr, K. Bolwin, W. Schnurnberger, M. Fischer, W. Neubrand, G. Eigenberger, Dynamic modelling and simulation of a polymer membrane fuel cell including mass transport limitation, *Int. J. Hydrogen Energy* 23 (3).
20. A. Rowe, X. Li, Mathematical modeling of proton exchange membrane fuel cells, *Journal of Power Sources* 102.
21. N. Djilali, D. Lu, Influence of heat transfer on gas and water transport in fuel cells, *Int. J. Therm. Sci.* 41.
22. T. Berning, D.M. Lu, N. Djilali, Three-dimensional computational analysis of transport phenomena in a pem fuel cell, *Journal of Power Sources* 106.
23. H. Ju, H. Meng, C.-Y. Wang, A single-phase, non-isothermal model for pem fuel cells, *International Journal of Heat and Mass Transfer* 48.
24. U. Pasaogullari, C.-Y. Wang, Two-phase transport and the role of micro-porous layer in polymer electrolyte fuel cells, *Electrochimica Acta* 49.
25. C. J. Bapat, S. T. Thynell, Anisotropic heat conduction effects in proton-exchange membrane fuel cell, *Journal of Heat Transfer* 129.
26. S. G. Kandlikar, Z. Lu, Thermal management issues in a pemfc stack – a brief review of current status, *Applied Thermal Engineering* 29.
27. J. Rumble (Ed.), *CRC Handbook of Chemistry and Physics*, 98th Edition, Taylor & Francis, 2017.
28. R. Bock, A. Shum, T. Khoza, F. Seland, N. Hussain, I. V. Zenyuk, O. S. Burheim, Experimental study of thermal conductivity and compression measurements of the gdl-mpc interfacial composite region, *ECS Transactions* 75 (14) (2016) 189–199.
29. O. S. Burheim, J. G. Pharoah, H. Lampert, P. J. S. Vie, S. Kjelstrup, Through-Plane Thermal Conductivity of PEMFC Porous Transport Layers, *J. Fuel Cell Sci. Technol.* 8 (2) (2011) 21013.
30. R. Taherian, A review of composite and metallic bipolar plates in proton exchange membrane fuel cell: Materials, fabrication, and material selection, *Journal of Power Sources* 265.
31. O. S. Burheim, G. Ellila, J. D. Fairweather, A. Labouriau, S. Kjelstrup, J. G. Pharoah, Ageing and thermal conductivity of Porous Transport Layers used for PEM fuel cells, *J. Power Sources* 221 (2013) 356–365.
32. O. Burheim, P. J. S. Vie, S. Møller-Holst, J. Pharoah, S. Kjelstrup, A calorimetric analysis of a polymer electrolyte fuel cell and the production of H<sub>2</sub>O<sub>2</sub> at the cathode, *Electrochim. Acta* 55 (3) (2010) 935–942.
33. S. M. Summer, S. Nicholson, Abusive testing of proton exchange membrane hydrogen fuel cells, *Tech. rep.*, U.S. Department of Transportation, Federal Aviation Administration (2016).